Interpreting Laser and Hot-Film Anemometer Signals in a Separating Boundary Layer

Roger L. Simpson*
Southern Methodist University, Dallas, Texas

RECENTLY an experimental study of a separating incompressible turbulent boundary layer produced by an adverse pressure gradient was completed.[1] A directionally sensitive fringe-type laser anemometer with a Bragg cell was used to measure the mean streamwise velocity U, the mean-square fluctuation $\bar{u}^2$, and the fraction of time the flow was moving in the downstream direction γ_p. In addition, a constant-temperature single-sensor cylindrical hot-film probe (Thermo-Systems, Inc., model 1274-10) was used to compare the behavior of this directionally insensitive sensor with the laser anemometer results. The purpose of the Note is to discuss the interpretation of signals from these two instruments in a separation region, i.e., when $\gamma_p < 1$.

Sampling spectrum analysis[2] of the laser anemometer signals was used because of the high-signal dropout level encountered in this flow with a relative low-particle seeding level and the high-signal frequencies produced by frequency shifting one incident beam. Most frequency trackers cannot handle either of these signal conditions. The signal from the photomultiplier tube or detector is input to a swept filter spectrum analyzer (HP 8558B). For each sweep of the analyzer when a particle (about 1 μ in size) is in the focal volume, a vertical voltage distribution proportional to the filter output is displayed. The simultaneous horizontal sweeping voltage is proportional to the signal frequency. The peak of the vertical voltage distribution marks the frequency of the passing particle signal and can be used as a gating signal to allow the instantaneous value of the horizontal sweep voltage to be sampled. This instantaneous voltage value is related to the instantaneous velocity U of the particle through the equation

$$U = \lambda_f [f_0 - w_0 + (\mathrm{df/de})E] = \lambda_v [f - w_0] \qquad (1)$$

where w_0 is the Bragg cell shifted frequency, f_0 is the analyzed frequency at the beginning of a sweep, $\mathrm{d}f/\mathrm{d}E$ is a constant relating the analyzed frequency to the horizontal sweep voltage, and E is the instantaneous horizontal sweep voltage.

Prior to gating the horizontal sweep voltage, the vertical voltage distribution is fed into a pulse-shaping circuit which produces a pulse simultaneously with the occurrence of the peak value. In the circuit used here, a 1-μsec-wide pulse is produced. This output pulse in used to trigger a sample-and-hold circuit, into which the horizontal sweep voltage has been input. The sampled sweep voltage E is held by the sample-and-hold circuit until a new signal from another particle is detected. The Applied University Research, Inc., Model 101 Signal Sampling System was used for these circuits. About 15-20 samples/sec were obtained. The output of the sampling interface circuit was input to a SAICOR Model 41 correlation and probability analyzer operated in the probability mode, obtaining a histogram of output voltages which is related to particle velocities through Eq (1). Each histogram was built over a record time of about 131 sec with a sampling time of 1 msec and was recorded using an x-y plotter.

Received April 2, 1975; revision received July 2, 1975. This work was sponsored by the U. S. Army Research Office Durham under Grant DAHC04-74-G-0024.

Index categories: Boundary Layers and Convective Heat Transfer-Turbulent; Lasers.

*Associate Professor Civil/Mechanical Engineering. Associate Fellow AIAA.

Figure 1 shows a typical histogram in the separated flow region. For frequencies greater than 25 MHz, the horizontal flow was downstream while lower frequencies corresponded to backflow upstream. The ratio of the histogram area for the downstream flow to the total histogram area is γ_p. The mean velocity U and mean-square fluctuation from the mean u^2 were determined directly from the histograms. The histograms were fairly well represented by a Gaussian distribution centered about the mean velocity. Thus, $u^2 \approx \sigma_u{}^2$, where σ_u is the standard deviation for the normal distribution.

Signal broadening effects on the mean-square fluctuation were found to be negligible. The "transit-time broadening," such as discussed by Johnson[3] for fringe systems, was determined by observing the width of the output histogram distribution produced in measuring the velocity on a spinning disk. This broadening was found to be less than or equal to the maximum system resolution (0.19 fps) or one bin of the digital probability analyzer. "Velocity gradient broadening" is produced in the presence of a transverse velocity gradient by the finite size of the focal volume diameter. The corrected mean-square fluctuation when $U >> (\bar{u}^2)^{1/2}$ is given by the equation presented by Goldstein and Hagen.[4]

To account for gradient broadening when $|\bar{U}| \leqslant (\bar{u}^2)^{1/2}$ as in a separating region, the fact that $\partial U/\partial y$ is not approximately constant with time must be considered. In the current method of signal processing, the discriminator level in the signal sampling system for the vertical output signal of the spectrum analyzer is set such that the random occurrence of particles whose signals are above that strength level pass through a smaller effective focal volume diameter d than the diameter at $1/e^2$ laser intensity locations, 0.0125 in. All these signals produce the same amplitude output from the pulse-shaping circuit, so each of these signals are treated equally. Thus, a top-hat type of particle location probability distribution should be used if the spatial probability of occurrence of a particle is the same everywhere within the effective focal volume. The apparent velocity probability distribution is given by

$$P_a(U) = \int_{U-(\partial U/\partial y)(d/2)}^{U+(\partial U/\partial y)(d/2)} \frac{P_r(\xi)\,\mathrm{d}\xi}{\{\partial \xi/\partial y\}d} \qquad (2)$$

where $P_r(\xi)$ is the true velocity probability distribution and ξ is a dummy velocity variable. The reasoning behind Eq. (2) is that if in a laminar flow, signals from $P_r(\xi)\mathrm{d}\xi$ particles were

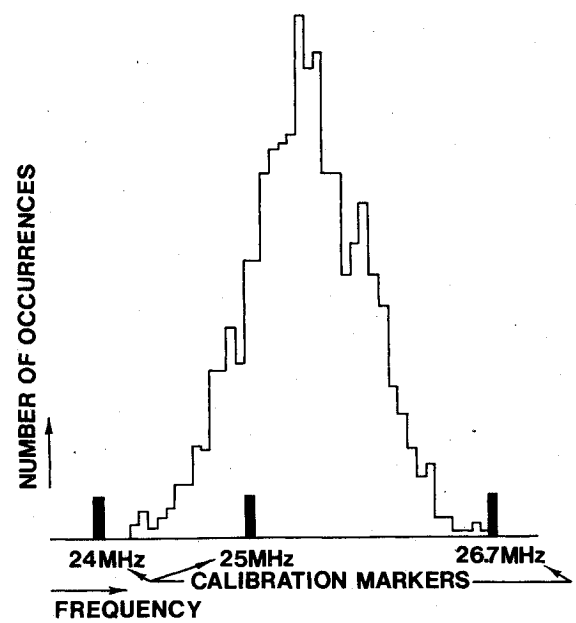

Fig. 1 Typical histogram of laser anemometer data samples in a separating flow. Zero velocity at the 25 MHz Bragg cell shifted frequency; positive velocities at higher frequencies.

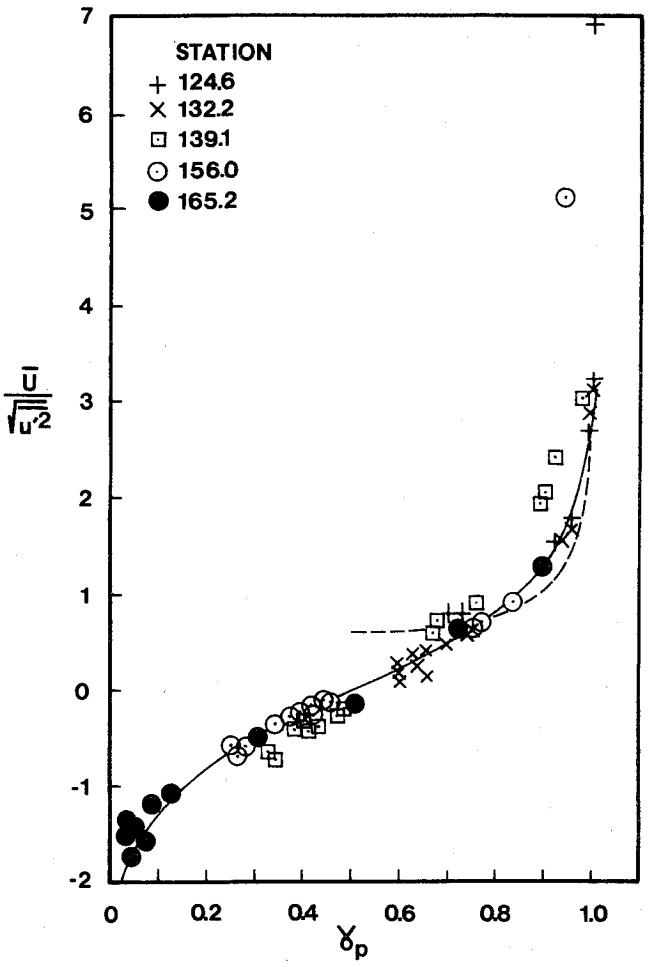

Fig. 2 Laser anemometer results of fraction of time the flow moves downstream γ_p as a function of $U/(\bar{u^2})^{1/2}$. Solid line, Eq. (3); dashed line, rectified Gaussian distribution model.

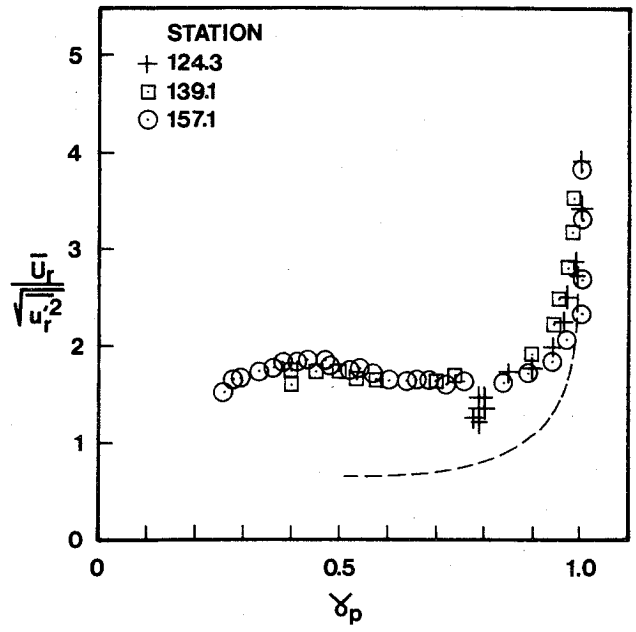

Fig. 3 γ_p as a function of $U_r/(\bar{u_r^2})^{1/2}$ from the hot-film anemometer. Dashed line, rectified Gaussian distribution model.

detected without gradient broadening, $P_a \equiv P_r$, while if gradient broadening were present, signals from the same number of particles would be spread over a top-hat profile $1/(\partial\xi/\partial y)d$ in amplitude. Using a Gaussian distribution for $P_r(\xi)$, Eq. (2) was evaluated. Only for the data very close to the wall (0.010 in. in this case) was the shape $P_a(U)$ determined to be appreciably different from $P_r(\xi)$. The corrected mean velocity was only about 5% greater than the apparent mean velocity while the corrected $(\bar{u^2})^{1/2}$ was about 5% less than the apparent value. Since the mean velocity quantity$(d/U)(\partial U/\partial y)$ is very small in the wall region of this separating flow, it appears unlikely that the instantaneous quantity $(\partial U/\partial y)(d/2U)$ would even be an order of magnitude larger and have appreciable effect on the apparent velocity probability distribution. Also note that γ_p is independent of gradient broadening since gradient broadening cannot change the direction of the apparent particle velocity.

It is difficult to justify the biasing correction of Tiederman et al.[5] for these data. This correction is due to the idea that higher velocity flow carries more particles through the focal volume per unit time, hence producing more signal pulses per unit time than slower flow. The apparent mean velocity would appear to be biased too high. However, since high-velocity signals spend less time in the focal volume of interest, the displayed peaks on the spectrum analyzer will be lower amplitude than for slower particles. Consequently, proportionately fewer higher velocity signals display peaks above a given amplitude discrimination level of the sampling system. Thus, these two effects tend to cancel in the present signal processing method, allowing one to neglect both. If the biasing correction was important here, then a dip should occur around the zero velocity value on each histogram, with higher histogram values occurring at greater speeds. This behavior was not observed on any of the histograms obtained.

Figure 2 shows experimental results for the fraction of time the flow moves downstream γ_p at a location plotted vs $U/(\bar{u^2})^{1/2}$ at the location from the laser anemometer signal histograms. Negative mean velocities correspond to backflow, in which case $\gamma_p < 1/2$. Also shown are the results from the equation

$$\gamma_p = 1/2 \left[1 + \mathrm{erf}\left(\frac{U}{(2\bar{u^2})^{1/2}} \right) \right] \tag{3}$$

which results when a Gaussian velocity probability distribution is used. The fact that all data from these experimental results are clustered about this equation suggests that the Gaussian distribution is not too crude a model.

The hot-film anemometer results $U_r/(\bar{u_r^2})^{1/2}$ are plotted vs γ_p in Fig. 3. Here the subscript r represents the fact that the hot-film sensor is directionally insensitive and interprets all cooling velocities as being positive, i.e., an effective rectification of backflow velocities. In addition to the probe calibration and linearization being questionable with rectification, the spanwise velocity and vertical velocity components are comparable to the streamwise velocity component, further increasing the uncertainty. However, for $\gamma_p > 0.8$ it was found that the mean velocity from the hot-film probe was essentially equal to that from the laser anemometer. For $\gamma_p < 0.95$, the hot-film $\bar{u_r^2}$ value was appreciably different from the laser anemometer result. If one simply rectifies the Gaussian probability distribution about the zero velocity line and computes the apparent mean velocity U_r and mean square u_r^2 values, neglecting all other components of the cooling velocity, the curve shown in Fig. 3 results. Only for γ_p near unity is this model crudely satisfied, indicating that the other previously mentioned effects are important. It appears that nearly all the data shown in Fig. 3 fall along a single path. However since $U_r/(\bar{u_r^2})^{1/2}$ is about the same for all $\gamma_p < 0.9$, one still cannot use this data correlation to determine γ_p from a hot-film measurement.

In conclusion, Eq. (3) describes the fraction of time a separated flow moves downstream in terms of the true streamwise mean and fluctuation velocities obtained from a directionally sensitive laser anemometer. This note also provides

useful information to re-evaluate existing hot-film and hot-wire measurements of separating turbulent boundary layers. For example, if the measured $U_r/(u_r^2)^{1/2}$ value was greater than 2, then $\gamma_p > 0.9$ and U_r should be valid. The u_r^2 values should only be trusted when $\gamma_p > 0.95$.

References

[1] Simpson, R.L., Strickland, J.H., and Barr, P.W., "Laser and Hot-Film Anemometer Measurements in a Separating Turbulent Boundary Layer," Rept. WT-3, Sept. 1974, Thermal and Fluid Sciences Center, Southern Methodist University, Dallas, Tex. available from NTIS: AD-A001115.

[2] Simpson, R.L. and Barr, P.W., "Laser Doppler Velocimeter Signal Processing Using Sampling Spectrum Analysis," *Rev. Sci. Instrum.*, Vol. 46, No. 7, July 1975, pp. 835-837.

[3] Johnson, D.A., "Insensitivity of Single Particle Time Domain Measurements to Laser Velocimeter 'Doppler Ambiguity'," *AIAA Journal*, Vol.11, June 1973, pp. 890-892.

[4] Goldstein, R.J. and Hagen, W.F., "Turbulent Flow Measurements Utilizing the Doppler Shift of Scattered Laser Radiation," *Physics of Fluids*, Vol. 10, June 1967, pp. 1349-1352.

[5] Tiederman, W.G., McLaughlin, D.K., and Reischman, M.M., "Individual Realization Laser-Doppler Technique Applied to Turbulent Channel Flow," presented at the *Third Biennial Symposium on Turbulence in Liquids*, University of Missouri—Rolla, Mo., Sept. 1973.

Technical Comments

Comment on "Buckling of Open Cylindrical Shells with Torsionally Stiff Rectangular Edge Stiffeners"

A.V. Viswanathan* and M. Tamekuni*
Boeing Commercial Airplane Company, Seattle, Washington

CLASSICAL theoretical solutions based on small deflection theory for buckling of open cylindrical shells (curved plates), both unstiffened and logitudinally stiffened and more general than that of Ref. 1, are available in literature.[2-6] References 2 and 3 and the associated computer program "BUCLAP2" consider curved laminates (with differing orthotropy directions in each lamina) subjected to combined inplane loads $\bar{N}_x$, $\bar{N}_y$, and $\bar{N}_{xy}$. Boundary conditions along the longitudinal sides can be arbitrary. While Refs. 4 and 5 present a unified analysis for longitudinally stiffened structures (open or closed) subjected to biaxial inplane loads, the algorithm of the associated computer program "BUCLASP2" takes advantage of "open" structures with open or closed stiffeners. The case of open cylindrical shells with torsionally stiff edge stiffeners thus become only a particular case of the more general solution. The analysis of Refs. 4 and 5 unlike that of Ref. 1 does not involve quantitative assumptions of the torsional stiffness or the lateral resistance of the stiffener and also does not ignore local stiffener deformations at buckling. Such deformations lower the effective stiffness of the stiffener, thereby further reducing the buckling loads.[7]

Reference 6 is an extension of Refs. 4 and 5 and presents an analysis for thermal stresses and buckling of heated logitudinally stiffened structures. While the temperature is uniform in the longitudinal direction, temperature variation in the cross-section is allowed. The analysis is also applicable to buckling of the structures described, with nonuniform loads in the cross-section, e.g. bending.

The formulation of Refs. 2 to 6 leads to a symmetric "buckling determinant." This enables the use of the algorithm of Ref. 8 which ensures that the lowest buckling load is determined with certainty and with few iterations. This method avoids the main disadvantages of the technique used in reference 1, namely, the risk of missing the lowest buckling load unless extremely small load increments are used and the consequent uneconomical computing time required.

The analysis of Refs. 9 to 12 are exact for prismatic flat plate structures. However, as discussed in Ref. 13, these methods can also be approximated with certain limitations to analyze open cylindrical shells, both unstiffened and longitudinally stiffened.

References

[1] Krishnamoorthy, G., "Buckling of Open Cylindrical Shells with Torsionally Stiff Rectangular Edge Stiffeners," *AIAA Journal*, Vol. 12, Oct. 1974, pp. 1348-1353.

[2] Viswanathan, A.V., Tamekuni, M., and Baker, L.L., "Elastic Stability of Laminated, Flat and Curved, Long Rectangular Plates Subjected to Combined Inplane Loads," NASA CR-2330, June 1974.

[3] Viswanathan, A.V., Tamekuni, M., and Baker, L.L., "Buckling Analysis for Anisotropic Laminated Plates Under Combined Loads," Paper 74-038, International Astronautical Federation, XXVth Congress, Amsterdam, Sept 30-Oct. 4, 1974.

[4] Viswanathan, A.V. and Tamekuni, M., "Elastic Buckling Analysis for Composite Stiffened Panels and Other Structures Subjected to Biaxial Inplane Loads," NASA CR-2216, Sept. 1973.

[5] Viswanathan, A.V., Tamekuni, M., and Tripp, Leonard L., "Elastic Stability of Biaxially Loaded Longitudinally Stiffened Composite Structures," *AIAA Journal*, Vol. 11, Nov. 1973, pp. 1553-1559.

[6] Viswanathan, A.V. and Tamekuni, M., "Analysis for Stresses and Buckling of Heated Composite Stiffened Panels and Other Structures, NASA CR-112227, March 1973.

[7] Stein, M. and Agarwal, B.L., personal communication, Sept. 1974, NASA, Langley Research Center, Hampton, Va.

[8] Wittrick, W.H. and Williams, F.W., "A General Algorithm for Computing Natural Frequencies of Elastic Structures," *Quarterly Journal of Mechanics and Applied Mathematics*, Vol. 24, Pt. 3, Aug. 1971, pp. 263-284.

[9] Williams, F.W. and Wittrick, W.H., "Numerical Results for the Initial Buckling of Some Stiffened Panels in Compression," *The Aeronautical Quarterly*, Vol. 23, Feb. 1972, pp. 24-40.

[10] Williams, F.W., Wittrick, W.H., and Plank, R.J., "Critical Buckling Loads of Some Prismatic Plate Assemblies," Presented at the *IUTAM Symposium on Buckling of Structures*, Harvard University, June 17-21, 1974.

[11] Williams, F.W. and Plank, R.J., "Critical Buckling of Some Stiffened Panels in Compression, Shear and Bending," *The Aeronautical Quarterly*, Vol. 25, Aug. 1974, pp. 165-179.

[12] Smith, C.S., "Bending, Buckling and Vibration of Orthotropic Plate Beam Structures," *Journal of Ship Research*, Vol. 12, No. 4, Dec. 1968, pp. 249-268.

[13] Williams, F.W., "Approximations in Complicated Critical Buckling and Free Vibration Analysis of Prismatic Plate Structures," *The Aeronautical Quarterly*, Vol. 25, Aug. 1974, pp. 180-185.

Received November 11, 1974; revision received December 20, 1974.
Index category: Structural Stability Analysis.

*Structures Staff. Member AIAA.

Reply by Author to A.V. Viswanathan and M. Tamekuni

G. Krishnamoorthy
San Diego University, San. Diego, Calif.

MOST of the references quoted in the discussion refer to the shell problems in which, the stifferners are

Received August 28, 1975.
Index category: Structural Stability Analysis.

*Professor, Department of Civil Engineering.